Plasticity more than (linear elastic crack) Propagation may govern standard Propagation Saw Test in snow: evidence from "Fracture toughness of mixed-mode anticracks in highly porous materials" experiments[1]

Hamed Haftbaradaran[1,2], Mahmood Heshmati[3], Nicola M. Pugno[1,4*]

[1] Mechano-X Labs, Department of Civil, Environmental, and Mechanical Engineering, University of Trento, Trento, 38123, Italy
[2] Department of Civil Engineering, University of Isfahan, Isfahan, Iran
[3] Department of Mechanical Engineering, Kermanshah University of Technology, Kermanshah, Iran
[4]School of Engineering and Materials Science, Queen Mary University of London, London, E1 4NS, UK

[*] Corresponding author: nicola.pugno@unitn.it
Emails of other authors: mahmood_heshmati1@yahoo.com; hamed.haftbaradaran@unitn.it

An extensive experimental campaign of propagation saw tests (PST) has recently been conducted, enabling systematic investigation of critical cut length vs. slope angle in snowpacks[1]. PST is considered crucial for understanding avalanche release. Using a linear elastic fracture mechanics (LEFM) framework built upon a linear elastic analysis, it was concluded that not a theoretical but a phenomenological mixed-mode fracture criterion governing fracture behavior of the weak layer can explain calculated energy release rates corresponding to experimental measurements.[1] In spite of this, we noted that while experiments presented a clear trend, the application of LEFM dispersed them, thus nor the theoretical nor the phenomenological approaches may result and indeed resulted in a good experimental comparison. Intrigued by this discrepancy, we show that strains at crack tip are indeed not consistent with linear elasticity for snow and instead that a simple and classical quadratic cap failure envelope combined with static equilibrium can explain results of these experiments once plastic (thus nonlinear) behavior of the weak layer under combined loading is considered. This is a natural consequence of the brittle-to-ductile transition, which is predicted by classical mechanics for any material by reducing the size scale,[2] thus failure of sufficiently "short" slabs of snow must be governed by plasticity rather than brittle fracture often considered in standard PST analyses. This finding builds on the original PST studies in snow suggesting such a transition at scales comparable to standard PST[3], as we have verified also calculating in a self-consistent manner the size of the plastic/cohesive zone: thus it is not surprising to us that at the length scale of standard (1 m) PSTs plastic/cohesive zone may dominate resulting in plastic failure and in general necessitating elasto-plastic more than linear elastic fracture mechanics. Summarizing our analysis highlights the importance of these complex measurements,[1] even if adopting a viewpoint different from the LEFM-based phenomenological interpretation,[1] by showing that they are very robust and that can be much better understood as a result of a simple nonlinear plastic behavior of the weak layer. This new interpretation (P=Plasticity more than Propagation in short PST) allows a simple extraction of the cap failure envelope parameters (critical stresses) for the weak layer from short PST (P=Plasticity, and suggests longer PST for extracting snow fracture properties, where P=Propagation), as we will hopefully adopt soon in Italy for better related avalanches forecasting.

Fig. 1(a) shows measurements of critical cut length (a) vs. slope angle (ϕ) which include 88 measurements on 9 days on snow slabs under three different levels of surface loading, a unique adjustable feature of the setup.[1] The figure shows a clear trend in the raw data specially for the downslope cuts, i.e. for $\phi > 0$. For the upslope cuts, $\phi < 0$, a somewhat mixed trend is found despite high controllability of the experiments. To interpret these results, following a common approach in avalanche mechanics, an elastic model was used with the snow slab treated as a Timoshenko beam resting on a linear elastic foundation which represents the weak layer. The model naturally requires numerical values of the elastic modulus of the snow as well as the normal and tangential stiffness constants of the elastic foundation. The model is then applied to the PST data using the measured critical cut length as an input to find the mode-specific energy release rates G_I and G_{II} for the cut (treated as a crack) predicted by LEFM, as shown in Fig. 1(b). Since the theoretical linear mixed mode criterion[4] of the type $(G_I/G_{Ic})+(G_{II}/G_{IIc})=1$ did not provide a satisfactory explanation, an empirical equation of the form $(G_I/G_{Ic})^m+(G_{II}/G_{IIc})^n=1$ was used, with exponents $m=5$, $n=2.2$, and the critical energy release rates $G_{Ic}=0.56\,\mathrm{J/m^2}$ and $G_{IIc}=0.79\,\mathrm{J/m^2}$ found as (four) fitting parameters.[1]

Matter Arising: P in these PSTs does not stand for Propagation.

Surprisingly, while the raw data in Fig. 1(a) show a clear trend, a large scatter appears in the calculated values of G_I and G_{II}. This holds regardless of the fracture criterion used, which for us hints at the inapplicability of the LEFM analysis.

Further, the values found for G_{Ic} and G_{IIc} [1] are nearly an order of magnitude larger than expected,[5] almost approaching that of ice.[6,7]

Note that the elastic model links the energy release rates to the stresses at the tip of the cut through Krenk's formula[8] as $G_I = t_{wl}(1-\nu_{wl}^2)\sigma_{tip}^2/(2E_{wl})$, $G_{II}=t_{wl}(1+\nu_{wl})\tau_{tip}^2/E_{wl}$, with $E_{wl}=0.15\,\mathrm{MPa}$, $\nu_{wl}=0.25$, and $t_{wl}=0.02\,\mathrm{MPa}$, being the Young's modulus, Poisson's ratio, and thickness of the weak layer, respectively. For $G_I=G_{Ic}$ and $G_{II}=G_{Ic}$, the normal and shear strains at failure can respectively be found from $\varepsilon_f=\sigma_{tip}(1-\nu^2)/E_{wl}$ and $\gamma_f=2\tau_{tip}(1+\nu)/E_{wl}$ as 1.9% and 3.6%, thus in a range where snow is not at all linear elastic. In fact, the calculated values of G_I in numerous cases vary between $G_{Ic} = 0.56\,\mathrm{J/m^2}$ and $0.9\,\mathrm{J/m^2}$, see Fig. 1(b), the latter corresponding to a normal strain of 2.4%. These strain ranges are too large for typical brittle materials as well as for snow and are reminiscent of ductile behavior. For example, Schöttner et al.[9] recently found far lower normal and shear strains of ~0.05% and ~0.12% at the corresponding peak stresses, and Schweizer[10] reports failure shear strains of below 0.3% for brittle fracture but ~3-4% for ductile behavior. The low brittle failure strain range is also consistent with numerical simulations.[11] This demonstrates that linear elasticity is not appropriate for these PST snow experiments[1]. So, how can we rationalize them?

Matter Resolved: P in these PSTs stands for Plasticity.

To provide an answer to this question, instead of using a LEFM model, we consider that the plastic strength of the weak layer under combined loading of a normal stress σ and a shear stress τ follows a classical cap failure envelope of the form $\left(\sigma/\sigma_{cr}\right)^2 + \left(\tau/\tau_{cr}\right)^2 = 1$, with σ_{cr} and τ_{cr} being the corresponding critical values.[12,13] A simple nonlinear plastic analysis suggests that failure along the entire weak layer happens when a uniform normal compressive/tensile stress and a uniform shear stress along the entire weak layer satisfy the cap failure criterion.[14] This is equivalent to a traction-separation law which captures perfectly plastic behavior of a cohesive interface under mixed mode loading.[15] Enforcing static equilibrium of the slab, one may find combinations of (σ, τ) corresponding to the measurements of Adam et al.[1] for which failure was recorded in PSTs. Normalized results reveal a clear trend as shown in Fig. 1(c) together with the simple cap failure envelope with σ_{cr} and τ_{cr} found from fitting.[14] Using a linear regression scheme on all 88 data points with σ^2 and τ^2 as dependent and independent variables, respectively, we found an R^2 of 0.38 which rises significantly to 0.47 once one outlier (relative to the same-day measurements) on Feb. 25 is excluded. The fitting yields cap failure parameters as $\sigma_{cr} = 2.32\,\mathrm{kPa}$, and $\tau_{cr} = 1.76\sigma_{cr}$. Exchanging dependent and independent variables in fitting yields $\sigma_{cr} = 2.57\,\mathrm{kPa}$, and $\tau_{cr} = 1.20\sigma_{cr}$ without changing R^2, see Appendix A. Note that the critical values of normal stress are comparable to the values reported by Reiweger et al.[13] and a ratio of 1.2 for τ_{cr}/σ_{cr} is very close to 1.23 found for one set of specimen by Chandel et al.[12] However, the interpretation here rests largely on the applicability of the cap model for $\sigma > 0.4\sigma_{cr}$, as shown in Fig. 1(c), and the value found for the cap model parameter τ_{cr} should not be interpreted as the true shear strength as in the low compressive stress regime a different failure envelope such as Mohr-Coulomb could practically dominate, lowering the true shear strength compared to the cap envelope.[13] However, PSTs remain outside this regime as the inclination angle remains well below 90°.

Instead, the quadratic failure envelope, $\sigma^2 + \beta_p \tau^2 = \sigma_{cr}^2$, $\beta_p = \left(\sigma_{cr}/\tau_{cr}\right)^2$, can interestingly be interpreted in terms of the mixed-mode cohesive interface model of Tvergaard and Hutchinson, see Appendix B.[15] This interpretation reveals a ratio of $\beta_p < 1$ as a signature of the facilitated normal, as compared to shear, deformation of the interface, here the weak layer. As shown in Appendix B, the associated flow rule with $\beta_p = 0.53$ explains deformation of the weak layer in compressive failure as measured through high-speed cameras combined with digital image correlation.[16] Therefore, the extracted values of $\beta_p = 0.32$ (or 0.69 depending on the fitting scheme) is consistent with the early-stage facile vertical collapse, but suppressed shear deformation, of a highly porous weak layer ahead of a PST cut.[16]

Since snow and weak layer properties could greatly vary from day to day, we repeated the same procedure above, allowing daily properties of the weak layer to be different. Results are shown in Fig. 1(d), now with R^2 exceeding 0.60 for all days. Note that a similar day-to-day treatment using LEFM[1] with a linear mixed-mode criterion and G_I, G_{II} as variables results in R^2 below 0.4 for all days except one, and a linear regression with G_I^5 and $G_{II}^{2.2}$ as variables based on the proposed nonlinear criterion does not improve this result, as we have verified.[14] In all cases, two fitting parameters were used for each day. Results based on the original model[14] with reduced tensile strength are included in Appendix C, exhibiting slight changes when the tensile strength is reduced by up to a factor of ~0.2. A reduced tensile strength results effectively in a larger tensile zone in the model.

We conclude that plastic collapse rather than brittle failure can more consistently explain PST measurements by Adam et al.[1] It can be shown that the load required for plastic failure of the weak layer falls below that required for fracture propagation in the weak layer once the slab length is small enough.[14] This is not surprising in the mechanics community and in accordance with the classical brittle-to-ductile transition that structural mechanics predicts for any material below a critical size threshold.[2] Our analysis demonstrates that the slab length of ~1 m used in standard PSTs could easily fall below the length required for brittle fracture to dominate.

To further check the plastic interpretation for these experiments, we calculate in a self-consistent manner the extension of the plastic/cohesive zone in the treated samples. We expect that the cohesive zone forming ahead of a cut can grow to cover the entire PST slab length. We scrutinized this point by developing a formulation based on the elastic foundation model which allows us to find the length of a cohesive zone ahead of a cut tip, see Appendix D. In accordance with the Dugdale model, we consider a cohesive zone of size δ ahead of a cut within which stress in the weak layer uniformly reaches the cohesive strength. δ is then found from requiring that stress in the weak layer ahead of the cohesive zone should relax to below the cohesive strength. The critical cut size in PSTs can then be interpreted as the cut size a in a long enough slab for which the cut together with the cohesive zone ahead of it essentially cover the length of a typical slab, i.e. $a+\delta=1\,\mathrm{m}$. As shown in Appendix D, the latter condition largely predicts the critical cut sizes measured by Adam et al.[1] As expected, the result demonstrates a large plastic/cohesive zone/length, in agreement with estimates of the cohesive zone size 0.5 to 1 m.[17]

The transition discussed here has been noted in the early PST developments, with transition lengths even exceeding 1 m.[3] The characteristic that distinguishes between the two failure regimes is that the critical cut length scales linearly with the slab length below a critical slab length, i.e. when plastic failure dominates, whereas the critical cut length approaches a constant independent of the slab length for long enough slabs, i.e. in the brittle failure regime. Therefore, slab lengths longer than typical ~1 m may be needed in PSTs if fracture properties of the weak layer are intended to be extracted. Fracture mechanics, not linear elastic but ideally viscous-plastic-elastic is relevant for real large-scale avalanches.

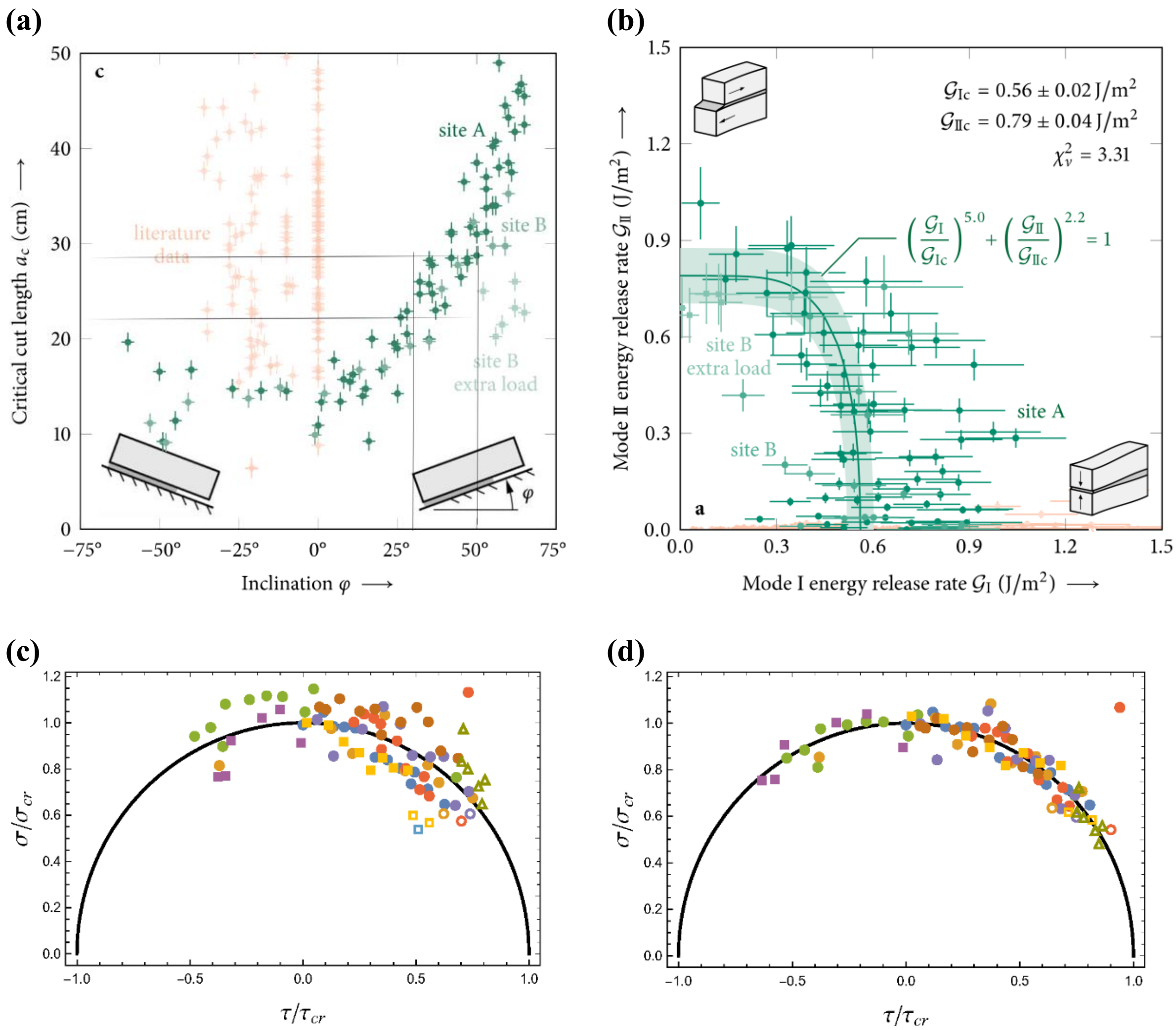

Fig. 1. (a) PST critical cut length measurements vs. slope angle showing a nearly clear trend (adapted from Adam et al.[1]); (b) Energy release rates calculated based on elastic model using LEFM show significant scatter, thus even the empirical fracture criterion represented by the curve (adapted from Adam et al.[1]) cannot provide a good experimental comparison; (c) Interpretation of test results using a simple nonlinear plastic analysis with the cap failure envelope fitted to all data points using σ_{cr} and τ_{cr} as fitting parameters; (d) Similar to (c) allowing σ_{cr} and τ_{cr} to vary for different days.

Acknowledgments: The authors acknowledge funding from the European Research Council (ERC) under the European Union's Horizon Europe research and innovation program (ERC-AdG-2024 FRAMEGLOW "Advanced quantized FRActure MEchanics models of ice and snow for GLObal Warming risk mitigation, Grant Agreement No. 101201568, PI Nicola M. Pugno).

Author contributions:

Methodology: HH, MH, NMP; Investigation: HH, MH; Visualization: HH;

Funding acquisition, Supervision: NMP; Writing – original draft, review & editing: HH, NMP, MH.

Competing interests: The authors declare that they have no competing interests.

References

1. Adam, V., Bergfeld, B., Weißgraeber, P., van Herwijnen, A. & Rosendahl, P. L. Fracture toughness of mixed-mode anticracks in highly porous materials. *Nat. Commun.* **15**, 7379 (2024).
2. Carpinteri, A. *Structural Mechanics: A Unified Approach*. (Chapman and Hall, London, 1997).
3. Gauthier, D. & Jamieson, B. Evaluation of a prototype field test for fracture and failure propagation propensity in weak snowpack layers. *Cold Reg. Sci. Technol.* **51**, 87–97 (2008).
4. Hutchinson, J. W. & Suo, Z. Mixed mode cracking in layered materials. *Adv. Appl. Mech.* **29**, 63–191 (1991).
5. Heierli, J., Gumbsch, P. & Zaiser, M. Anticrack nucleation as triggering mechanism for snow slab avalanches. *Science (80-.).* **321**, 240–243 (2008).
6. Andrews, E. H. & Lockington, N. A. The cohesive and adhesive strength of ice. *J. Mater. Sci.* **18**, 1455–1465 (1983).
7. Nixon, W. A. & Schulson, E. M. A micromechanical view of the fracture toughness of ice. *Le J. Phys. Colloq.* **48**, C1-313-C1-319 (1987).
8. Krenk, S. Energy release rate of symmetric adhesive joints. *Eng. Fract. Mech.* **43**, 549–559 (1992).
9. Schöttner, J. *et al.* Testing the Strength of Buried Surface Hoar Weak Layers Under Combined Compression and Shear Loading. *Geophys. Res. Lett.* **53**, (2026).
10. Schweizer, J. Laboratory experiments on shear failure of snow. *Ann. Glaciol.* **26**, 97–102 (1998).
11. Chandel, C., Srivastava, P. K. & Mahajan, P. Determination of failure envelope for faceted snow through numerical simulations. *Cold Reg. Sci. Technol.* **116**, 56–64 (2015).
12. Chandel, C., Mahajan, P., Srivastava, P. K. & Kumar, V. The behaviour of snow under the effect of combined compressive and shear loading. *Curr. Sci.* 888–894 (2014).
13. Reiweger, I., Gaume, J. & Schweizer, J. A new mixed-mode failure criterion for weak snowpack layers. *Geophys. Res. Lett.* **42**, 1427–1432 (2015).

14. Haftbaradaran, H., Heshmati, M. & Pugno, N. M. Plastic more than brittle failure may govern standard propagation saw tests. at https://doi.org/10.31223/X5XZ26 (2026).

15. Tvergaard, V. & Hutchinson, J. W. The influence of plasticity on mixed mode interface toughness. *J. Mech. Phys. Solids* **41**, 1119–1135 (1993).

16. Bergfeld, B. *et al.* Signatures of the sub-Rayleigh to supershear fracture transition in snow avalanche experiments. *Nat. Commun.* **16**, 11153 (2025).

17. McClung, D. M. & Schweizer, J. Fracture toughness of dry snow slab avalanches from field measurements. *J. Geophys. Res. Earth Surf.* **111**, (2006).

Appendix A: *Linear regression model based on exchanging dependent and independent variables*

Using linear regression, one may exchange the dependent and independent variables. Treating τ^2 as a linear function of σ^2 (referred to as the fitting scheme II), instead of the opposite (scheme I), values of τ_{cr}^2 and $\left(\tau_{cr}/\sigma_{cr}\right)^2$ can be inferred. It turns out that while the two schemes yield somewhat different values for the model parameters, the resulting R^2 remains unchanged. Table A1 below shows how the inferred values of the model parameters change adopting the two schemes. In particular, the deduced value of σ_{cr} increases and τ_{cr}/σ_{cr} decreases in the second scheme. The value of 1.76 found for the latter from global fitting reduces to 1.20, and its daily range of 1.24-1.93 reduces to 1.16-1.56 once the second scheme is used. The normalized results are illustrated in Fig. A1(a) for global fitting and in Fig. A1(b) for daily, with τ/τ_c and σ/σ_c shown respectively on the vertical and horizontal axes to reflect the fact that τ^2 has been treated as a function of σ^2. Minimizing an error measure defined with respect to both variables simultaneously would lead to a slightly different result, at a price of a much larger complexity of the procedure.

Table A1. Results based on exchanging dependent and independent variables in linear regression in comparison to the first scheme; 95% confidence intervals are also provided.

	Fitting scheme I		Fitting scheme II				
	σ_{cr} (kPa)	τ_{cr}/σ_{cr}	σ_{cr} (kPa)	τ_{cr} (kPa)		τ_{cr}/σ_{cr}	
					95% CI		95% CI
All data	2.31	1.85	2.63	3.00	(2.73-3.27)	1.14	(0.98-1.29)
outlier removed	2.32	1.76	2.57	3.09	(2.84-3.33)	1.20	(1.05-1.33)
Feb. 18	2.32	1.36	2.34	3.07	(2.81-3.31)	1.31	(1.17-1.44)
Feb. 23	2.22	1.79	2.39	3.33	(2.39-4.05)	1.39	(0.74-1.82)
Feb. 24	2.57	1.45	2.62	3.38	(2.72-3.94)	1.29	(0.99-1.54)
Feb. 25	2.24	2.32	2.41	2.45	(0.96-3.34)	0.72	(0-1.28)
outlier removed	2.46	1.29	2.52	3.04	(2.73-3.32)	1.20	(1.02-1.37)
Mar. 02	2.36	1.71	2.50	3.54	(2.86-4.11)	1.41	(0.99-1.74)
Mar. 03	2.50	1.93	2.59	4.04	(2.98-4.87)	1.56	(1.05-1.94)
Mar. 08	2.25	1.24	2.30	2.66	(2.34-2.94)	1.16	(0.96-1.32)
Mar. 09	2.36	1.02	2.49	2.03	(0.94-2.72)	0.82	<1.17
Mar. 10*	3.13	1.22	3.75	3.53	(2.99-4.00)	0.94	<1.37

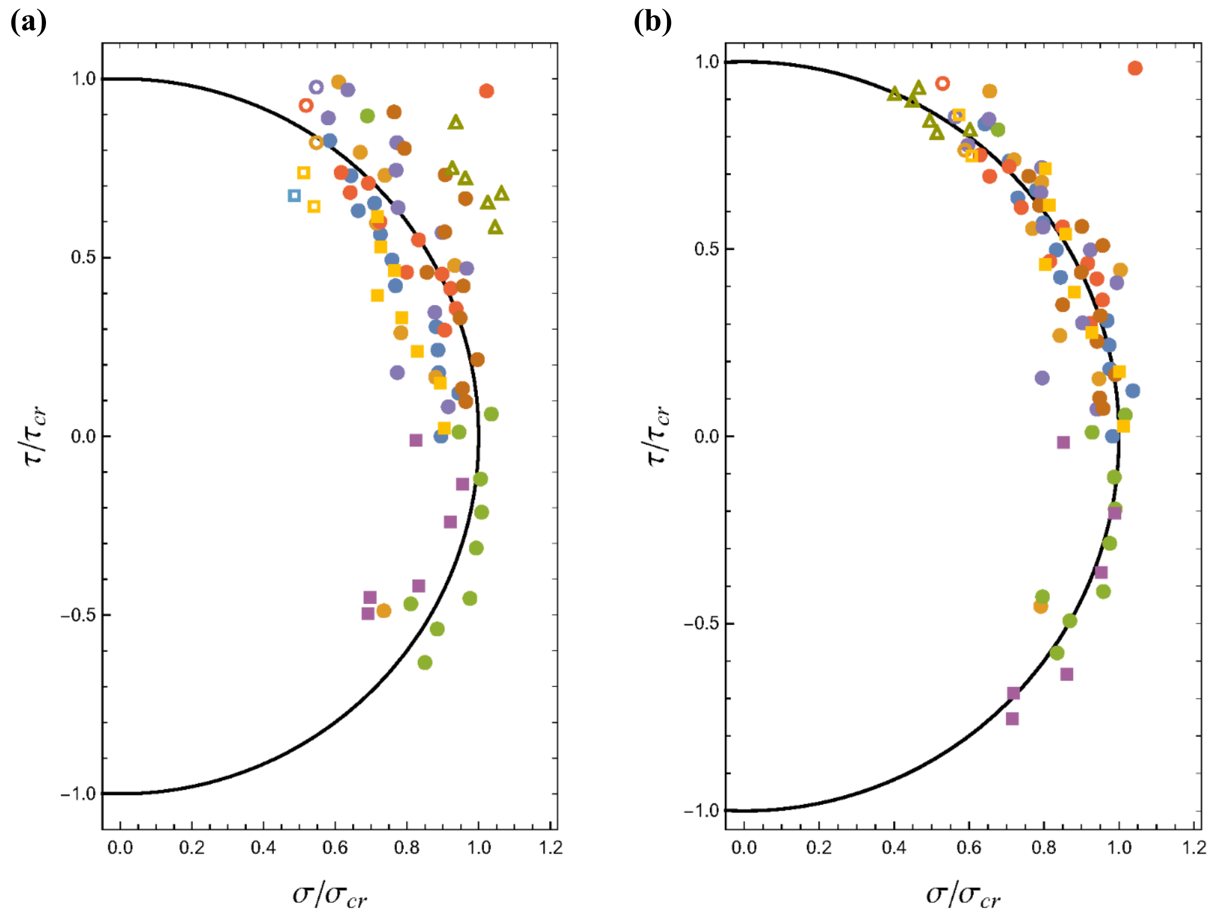

Fig. A1. Fitting results using linear regression with τ^2 as the dependent and σ^2 as the independent variables: (a) global fitting, or (b) daily fitting.

Appendix B: *Interpretation in terms of the mixed mode cohesive interface model*

The yield surface used for the weak layer in this work is of the form $\sigma^2 + \beta_p \tau^2 = \sigma_{cr}^2$, $\beta_p = \left(\sigma_{cr}/\tau_{cr}\right)^2$. This behavior can be examined in the light of the mixed-mode cohesive interface model of Tvergaard and Hutchinson[15]. Using a traction potential, they[15] derive traction-separation laws of the form

$$\sigma = \frac{\sigma_e(\lambda)}{\lambda}\frac{\delta_n}{\delta_{n0}}, \; \tau = \frac{\sigma_e(\lambda)}{\lambda}\frac{\delta_{n0}}{\delta_{t0}}\frac{\delta_t}{\delta_{t0}}, \tag{B1}$$

where $\lambda = \sqrt{\left(\frac{\delta_n}{\delta_{n0}}\right)^2 + \left(\frac{\delta_t}{\delta_{t0}}\right)^2}$ is a deformation measure, with δ_{t0} and δ_{n0} being respective reference values of the tangential and normal displacement jump across the interface, denoted by δ_t and δ_n. Here, $\sigma_e(\lambda)$ is the effective stress measure which describes plastic flow of the interface. Inserting Eq. (B1) into $\sigma^2 + \beta_p \tau^2 = \sigma_{cr}^2$, setting $\sigma_e(\lambda) = \sigma_{cr}$, results in

$$\lambda^2 = \left(\frac{\delta_n}{\delta_{n0}}\right)^2 + \beta_p \left(\frac{\delta_{n0}}{\delta_{t0}}\right)^2 \left(\frac{\delta_t}{\delta_{t0}}\right)^2.$$

Comparing this to the deformation measure $\lambda = \sqrt{\left(\frac{\delta_n}{\delta_{n0}}\right)^2 + \left(\frac{\delta_t}{\delta_{t0}}\right)^2}$, suggests $\beta_p = \left(\frac{\delta_{t0}}{\delta_{n0}}\right)^2$. As noted by Tvergaard and Hutchinson,[15] a value of $\frac{\delta_{t0}}{\delta_{n0}} < 1$ suggests that shear deformation of the interface is suppressed relative to the normal deformation. This can be seen from Eq. (B1) which suggests

$$\frac{\delta_t}{\delta_n} = \beta_p \frac{\tau}{\sigma}. \tag{B2}$$

It is of interest to examine this relation in the light of weak layer deformation measurements.[16] Using high-speed cameras combined with digital image correlation to capture deformation of the weak layer as it collapses following introduction of a PST cut, it was found that closer to the cut tip (close-up #1 in their experiments), a compressive failure mode dominates resulting in the volumetric collapse of the weak layer.[16] In this mode, slope-normal displacement of the weak layer initially increases to ~5.5 mm almost in linear proportion to the slope-parallel displacement reaching ~2.2 mm. Their measurement is for a slope angle of $\phi = 37^\circ$. Inserting $\frac{\tau}{\sigma} \approx \tan\phi$, with $\delta_t = 2.2\,\text{mm}$, and $\delta_n = 5.5\,\text{mm}$ into Eq. (B2), results in $\beta_p = 0.53$. A value of $\beta_p < 1$ found from our fittings (i.e. 0.32 or 0.69 depending on the fitting scheme) is hence consistent with early-stage volumetric collapse of the porous weak layer in the slope-normal direction as characterized by experiments.[16]

Appendix C: *Results for different choices of* α *(reduced tensile strength)*

To examine how a choice of α smaller than 1 could affect results, we also performed similar analyses by reducing α in the original model.[14] The resulting values of R^2 are summarized in Table C1 for $\alpha = 1$, 0.5 and 0.2 with the corresponding values of the fitting parameters given in Table C2. Reducing α to 0.2, the R^2 reduces to ~0.49 and to ~0.53 for two days but remains larger than 0.6 for other days varying only marginally. Both σ_{cr} and τ_{cr}/σ_{cr} exhibit only slight changes as α reduces to 0.2, see Table C2. Note that a choice of $\alpha = 0.2$ corresponds to a tensile yield strength of ~0.45-0.52 kPa which is comparable to ~0.4 kPa as reported by Reiweger et al.[13] Normalized results with $\alpha = 0.5$ are shown in Fig. C1 and with $\alpha = 0.2$ in Fig. C2. Fig. C1(a) and C2(a) show results of global fitting to all measurements, and Fig. C1(b) and C2(b) results of daily fitting. We conclude that the plastic failure model exhibits consistency with the experiments for a large range of values of α from 1 down to ~0.2. Reducing α to below ~0.2 resulted in departure form the model with reduced R^2. In effect, a reduced tensile strength increases the required size of the tensile zone for maintaining the slab equilibrium. When a very small α is considered in the model, the model prediction of a large tensile zone is physically equivalent to the nucleation of a large crack over the considered "tensile" zone. This happens in particular for upslope cuts ($\phi < 0$) at large slope angles where a large "tensile" zone is predicted at the top (far) end of the slab.

Table C1. Effect of α on R^2.

	Number of tests	R^2		
		$\alpha=1$	$\alpha=0.5$	$\alpha=0.2$
All data	88	0.38	0.37	0.36
outlier removed	87	0.47	0.46	0.44
1 (Feb 18)	12	0.92	0.92	0.92
2 (Feb 23)	9	0.61	0.62	0.63
3 (Feb 24)	10	0.79	0.75	0.53
4 (Feb 25)	12	0.10	0.08	0.06
outlier removed	11	0.87	0.87	0.87
5 (Mar 02)	11	0.69	0.68	0.67
6 (Mar 03)	11	0.66	0.63	0.61
7 (Mar 07)	1			
8 (Mar 08)	10	0.88	0.87	0.87
9 (Mar 09)	6	0.64	0.58	0.49
10 (Mar 10)	6	0.60	0.60	0.60

Table C2. Model parameters extracted from fitting with different values of α: the first row for global fittings and the subsequent rows for daily fitting.

	Number of tests	$\alpha=1$		$\alpha=0.5$		$\alpha=0.2$	
		$Y=\sigma_{cr}$ (kPa)	$\frac{\tau_{cr}}{\sigma_{cr}}$	$Y=\sigma_{cr}$ (kPa)	$\frac{\tau_{cr}}{\sigma_{cr}}$	$Y=\sigma_{cr}$ (kPa)	$\frac{\tau_{cr}}{\sigma_{cr}}$
All data	88	2.31	1.85	2.33	1.83	2.35	1.81
Outlier removed	87	2.32	1.76	2.34	1.74	2.36	1.71
1 (Feb 18)	12	2.32	1.36	2.32	1.36	2.33	1.35
2 (Feb 23)	9	2.22	1.79	2.23	1.77	2.24	1.75
3 (Feb 24)	10	2.57	1.45	2.61	1.48	2.67	1.57
4 (Feb 25)	12	2.24	2.32	2.24	2.39	2.23	2.50
Outlier removed	11	2.46	1.29	2.47	1.28	2.47	1.28
5 (Mar 02)	11	2.36	1.71	2.37	1.70	2.38	1.69
6 (Mar 03)	11	2.50	1.93	2.52	1.93	2.53	1.93
7 (Mar 07)	1						
8 (Mar 08)	10	2.25	1.24	2.26	1.23	2.27	1.22
9 (Mar 09)	6	2.36	1.02	2.38	1.06	2.40	1.12
10 (Mar 10)	6	3.13	1.22	3.13	1.22	3.13	1.22

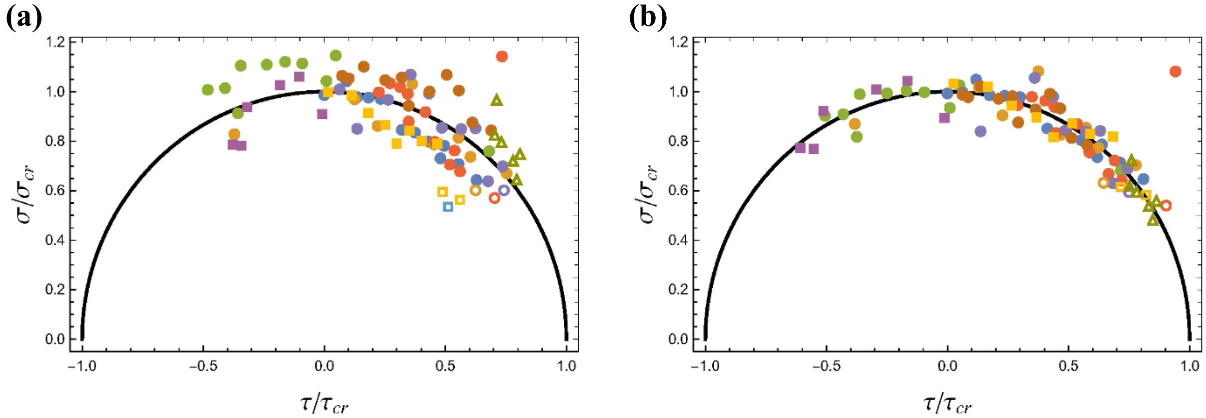

Fig. C1. Fitting results with $\alpha = 0.5$ based on (a) global fitting, or (b) daily fitting.

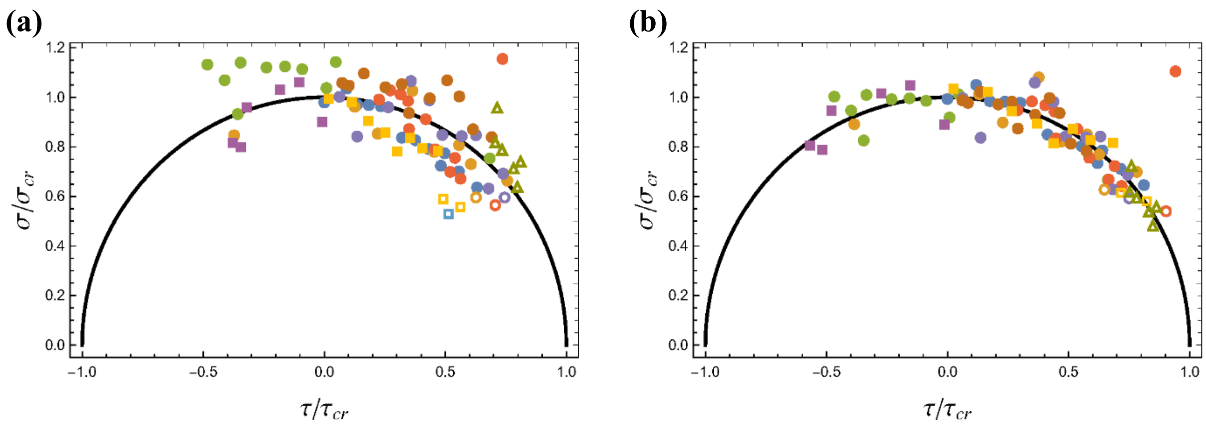

Fig. C2. Fitting results with $\alpha = 0.2$ based on (a) global fitting, or (b) daily fitting.

Appendix D: *Prediction of the size of the process (plastic/cohesive) zone*

The beam on elastic foundation model can be used to calculate the length of the process zone ahead of a cut. Suppose that a downslope cut of length a is made in a PST. We consider formation of a process or cohesive zone of length δ ahead of the cut tip. A coordinate system is introduced with its origin at the tip of the cohesive zone, hence the weak layer is behaving elastically within $x < 0$, the cohesive zone spans within $0 < x < \delta$, and the cut within $\delta < x < \delta + a$. Note that we have assumed that the slab is indefinitely extended in the negative x direction. In accordance with the Dugdales's notion of cohesive zone, we assume a uniform cohesive compressive stress σ_{coh} by the weak layer on the slab within $0 < x < \delta$. Using the Euler-Bernoulli beam theory, deformation of the slab can be found by solving the following equations,

$$E'\overline{I}\,\frac{d^4 w_1(x)}{dx^4} + k_n w_1(x) = \gamma_n\,, \quad x < 0\,, \tag{D3}$$

$$E'\overline{I}\,\frac{d^4 w_2(x)}{dx^4} = \gamma_n - \sigma_{coh}\,, \quad 0 < x < \delta\,, \tag{D4}$$

$$E'\overline{I}\,\frac{d^4 w_3(x)}{dx^4} = \gamma_n\,, \quad \delta < x < \delta + a\,, \tag{D5}$$

where $E' = \dfrac{E}{1-\nu^2}$ is the plane strain modulus of the slab, E and ν being respectively elastic modulus and Poisson's ratio, $\overline{I} = H^3/12$ its cross-sectional moment of inertia (per unit slab width), k_n normal stiffness of the weak layer, and γ_n distributed normal load on the slab. Here, $w_1(x)$, $w_2(x)$, and $w_3(x)$ represent vertical deformation of the beam within the three regions. Solutions to Eqs. (D3)-(D5) can be written as

$$w_1(x) = a_1 e^{\lambda x}\cos\lambda x + b_1 e^{\lambda x}\sin\lambda x + \frac{\gamma_n}{k_n}\,, \tag{D6}$$

$$w_2(x) = a_2 x^3 + b_2 x^2 + c_2 x + d_2 + \frac{\lambda^4}{6k_n}\left(\gamma_n - \sigma_{coh}\right), \tag{D7}$$

$$w_3(x) = a_3 x^3 + b_3 x^2 + c_3 x + d_3 + \frac{\lambda^4}{6k_n}\gamma_n\,. \tag{D8}$$

where $\lambda = \left(\dfrac{k_n}{4E\overline{I}}\right)^{1/4}$, and a_i, b_i, c_i, and d_i are unknown constants. In writing Eq. (D6), we have invoked the condition that $w_1(x)$ should remain bounded as $x \to -\infty$. Eqs. (D3)-(D5) should be solved subject to the continuity of the deformation, slope, shear force and bending moment in the beam at $x = 0$ and $x = \delta$, and the free boundary conditions at the endpoint, $x = a + \delta$, i.e. zero shear force and bending moment. The total of 10 conditions stated can be used to compute the 10 unknown constants, a_i, b_i, c_i, and d_i in Eqs. (D6)-(D8). In particular, the stress at the common tip of the elastic zone and cohesive zone, i.e. at $x=0$, is found as

$$\sigma(x=0)=\gamma_n\left(1+a\lambda+\delta\lambda\right)^2-\lambda\delta\left(2+\lambda\delta\right)\sigma_{coh}. \tag{D9}$$

The cohesive zone size δ can be found by requiring that the stress in the elastic part of the weak layer falls below the cohesive strength. Hence, we set

$$\sigma(x=0)=\sigma_{coh}, \tag{D10}$$

which results in

$$\delta=\frac{1-\sqrt{\dfrac{\gamma_n}{\sigma_{coh}}}\left(1+\lambda a\right)}{\left(\sqrt{\dfrac{\gamma_n}{\sigma_{coh}}}-1\right)\lambda}. \tag{D11}$$

Note the special case of $\delta\to\infty$ for $\gamma_n\to\sigma_{coh}$. Further, note that for $a=0$, Eq. (D11) gives a nonphysical negative value for δ, implying that a cohesive zone forms only for a minimum cut size $a_{\min}$ which can be found by setting $\delta=0$ as $a_{\min}=\frac{1}{\lambda}\left(\sqrt{\frac{\sigma_{coh}}{\gamma_n}}-1\right)$. The latter relation implies that a cohesive zone forms in the absence of a cut only when the loading reaches the cohesive strength, i.e. $a_{\min}=0$ for $\gamma_n=\sigma_{coh}$.

As an example, Adam et al.[1] have reported a critical cut size of $a=10.9\,\text{cm}$ for a flat slab $\phi=0$ under an overall distributed load of $\gamma_n=1815\,\text{N/m}^2$ (surface load plus slab weight). Since they use a slab length of 1 m in their test, it is of interest to ask for what cohesive strength of the weak layer the cohesive zone grows to the end of the slab. Inserting $\delta=L-a=0.891\,\text{m}$, with $E=30\,\text{MPa}$, $H=11.5$ cm, $\nu=0.25$, $E_{wl}=0.15\,\text{MPa}$, $t_{wl}=2\,\text{cm}$ into Eq. (D11), one arrives at a cohesive strength of $\sigma_{coh}\approx 2.19\,\text{kPa}$. This result is very close to the cohesive strength of $Y=\sigma_{cr}=2.31\,\text{kPa}$ found from fitting the plastic collapse model to all PST measurements.[14] If we use the latter cohesive strength, we find $\delta=0.64\,\text{m}$ based on the estimate for an infinitely long flat slab.

Extension for a sloped surface

For a sloped slab of snow, with the inclination angle ϕ, the tangential component of loading as well as the shear stress at the weak layer result in a distributed moment on the beam which can be accounted for using the Euler-Bernoulli theory, as in Appendix C of Haftbaradaran et al.[14] Following the same approach as above, the size of the cohesive zone is found as

$$\hat{\delta} = \frac{\hat{\gamma}_n\left(1+\hat{a}-\hat{\mu}_0\tan\phi\right)-1+\sqrt{\hat{\gamma}_n\left(\hat{a}^2+(\hat{\mu}_0\tan\phi)^2\hat{\gamma}_n-2\hat{a}\tan\phi\left(\hat{\gamma}_n\hat{\mu}_0+\hat{\mu}_1-\hat{\gamma}_n\hat{\mu}_1\right)\right)}}{1-\hat{\gamma}_n}, \qquad \text{(D12)}$$

where $\hat{\delta}=\lambda\delta$, $\hat{a}=\lambda a$, $\hat{\mu}_0=\lambda\mu_0$, $\hat{\mu}_1=\lambda\mu_1$, $\hat{\gamma}_n=\frac{\gamma_n}{\sigma_{coh}}$ are dimensionless parameters with

$\mu_0=\frac{H}{2}+e$ and $\mu_1=e$ being eccentricity parameters, $e=\frac{p_{surf}H}{2(p_{surf}+\rho gH)}$, and p_{surf} being the applied surface load. Note that Eq. (D12) reduces to Eq. (D11) for $\phi=0$, and diverges as $\hat{\gamma}_n\to 1$.

With the cohesive zone size given by (D12), one may find a cut size a for which the cut and the cohesive zone formed ahead of it together span a length of 1 m, enough to cover an entire typical slab in PST experiments. Since there is already on average a shear stress of $\tau=\frac{\gamma\sin\phi}{1-a/L}$ (γ being the distributed vertical load) on the weak layer in a finite slab of length L, we use $\sigma_{coh}=\sqrt{Y^2-\beta_p\tau^2}$ for the normal cohesive strength. Predictions of the critical cut size a for which $a+\delta=1\,\text{m}$ are given in Fig. D1 and compared to the 65 experiments carried out on 6 days under the same applied load.[1] These predictions have been found using $Y=2.41\,\text{kPa}$ and $\beta_p=0.42$, which are the average values of these parameters previously found for the same 6 days based on the plastic failure model,[14] hence no fitting parameter has been used here. All other material parameters are taken as stated before. As shown in Fig. D1, the infinite-slab solution based on Eq. (D12) exhibits a good agreement with the experimental measurements ($R^2=0.77$), although expectably slightly overestimates them.

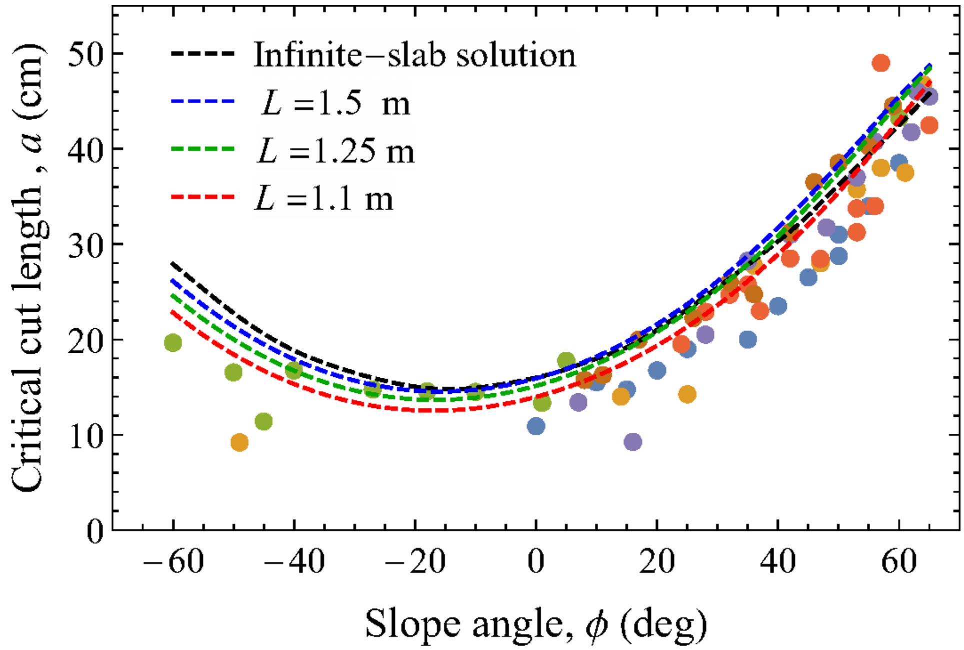

Fig. D1. Prediction of the critical cut length as the cut size for which the cut together with the cohesive zone ahead of it reaches 1 m, and comparison with experiments on 6 days.

While the infinite-slab problem allows derivation of a closed-form analytical solution for the cohesive zone size, one in fact can use the same method for a slab of a finite length. This can be achieved by replacing Eq. (D6) with the complete solution which is in the form

$$w_1(x) = a_1 e^{\lambda x}\cos\lambda x + b_1 e^{\lambda x}\sin\lambda x + c_1 e^{-\lambda x}\cos\lambda x + d_1 e^{-\lambda x}\sin\lambda x + \frac{\gamma_n}{k_n}, \tag{D13}$$

and enforcing the conditions of zero shear force and bending moment at the slab endpoint at $x = -(L-\delta)$ to enable determination of the two additional unknowns c_1 and d_1. For a finite slab, the bonded weak layer is in fact subject to a shear stress that is on average larger than that in an infinite slab by a factor of $\dfrac{1}{(1-a/L)}$ resulting in an increased distributed moment on the slab.[14] This results in an increased eccentricity $\mu_0 = \dfrac{H}{2(1-a/L)} + e$ when the slab length is finite. The size of the cohesive zone can still be found from enforcing Eq. (D10). We used this method to numerically find the cut size a for which $a+\delta$ reaches 1 m for finite values of L, and the results are included in Fig. D1. To examine how predictions found for finite slab lengths deviate from those based on the infinite-slab solution, we have presented results for slab lengths of $L = 1.5\,\mathrm{m}$, $1.25\,\mathrm{m}$ and $1.1\,\mathrm{m}$ approaching but remaining larger than $a + \delta = 1\,\mathrm{m}$. Note that the present formulation is not applicable at the limit of $L = a + \delta$ as this is equivalent to a vanishing elastic zone. The results shown are in very good agreement with the experiments, with R^2 between 0.75 and 0.88.

A couple of points are however noteworthy for the analysis of finite-sized slabs. The analysis here assumes formation of a single cohesive zone from the cut tip and does not account for the development of a cohesive zone from the other end of the slab. While the effect of this second process zone could be negligible for a long enough slab, it could influence the results found here for finite-sized slabs with the expectable result of further lowering the critical cut size. In particular, as also revealed by the plastic failure analysis,[14] equilibrium considerations under certain conditions require the weak layer to withstand tensile stresses. Therefore, the analysis here is to be further extended to account for the limited tensile strength of the weak layer. However, the present analysis demonstrates that formation of the cohesive zone from the cut tip is a dominant factor in determining the critical cut size for failure.